ELSEVIER

PII: S0032-3861(97)00474-6

Polymer Vol. 39 No. 12, pp. 2409–2414, 1998

0032-3861/98/$19.00+0.00

Application of a CCD-Based X-ray diffractometer to polymer fibre diffraction

S. Hanna*, A. M. E. Baker and A. H. Windle
Department of Materials Science and Metallurgy, University of Cambridge, Pembroke Street, Cambridge CB2 3QZ, UK
(Received 20 January 1997; revised 21 April 1997)

A new diffractometer has been built incorporating a small-area charge-coupled device (CCD) as the X-ray detector. The diffractometer is suitable for studying uniaxially oriented polymer fibres, and produces high resolution fibre diffraction data considerably faster than is possible using a conventional scintillation counter. The sample and detector are mounted on a 3-circle goniometer, and a fibre pattern is constructed from a series of separate diffraction 'snapshots', each centred on a different point in reciprocal space. The advantages of the new system are the ability: (1) to produce an undistorted representation of the fibre diffraction pattern; and (2) to access reflections close to the reciprocal fibre axis which are often missing from normal incidence X-ray fibre diffraction photographs. These features make it particularly useful for studying diffuse scattering from partially ordered materials. The operation of the diffractometer is demonstrated using fibres of polyethylene, polypropylene and a copolymer of 1.4-hydroxybenzoic acid with 2,6-hydroxynaphthoic acid. In the latter case a detailed examination of the shapes of the meridional reflection is possible, demonstrating them to be consistent with predictions from current crystallization theories. The effect of imperfect molecular orientation on the appearance of the fibre diffraction patterns is also discussed.

(Keywords: polymer fibre diffractometer; area detector; charge-coupled device)

INTRODUCTION

When performing structural studies of polymers, it is always desirable to obtain high-resolution fibre diffraction data from as large a region of reciprocal space as possible. In this respect,traditional methods of data collection, involving X-ray film or conventional fibre diffractometry, have drawbacks. X-ray film has a poor dynamic response, yields only semi-quantitative peak intensities, and, due to the curvature of the Ewald sphere, gives a limited and distorted view of reciprocal space[1]. Diffractometry, on the other hand, while allowing a more complete coverage of reciprocal space, can be extremely slow, typically requiring days or weeks for data collection from oriented amorphous polymers[2,3]. Thus, to extend diffractometry to the resolution required for crystalline samples implies prohibitively long measurement times when using conventional laboratory X-ray sources.

We have addressed these problems by building a new fibre diffractometer, which incorporates a small-area X-ray detector instead of a single-point detector. The area detector is of the television type[4,5], in which the active element is a charge-coupled device (CCD) fitted with a scintillator and an optical image intensifier. The CCD camera is mounted on a three-circle goniometer, allowing a succession of diffraction images to be obtained centred on different points in reciprocal space. Each image is subsequently transformed into linear reciprocal space coordinates and a composite undistorted section through cylindrically-averaged reciprocal space is created.

* To whom correspondence should be addressed. Present address: H. H. Wills Physics Laboratory, University of Bristol, Tyndall Avenue, Bristol, BS8 1TL, UK

Much of the development work for this system has been published already[6,7], and we shall only briefly review it here. The aim of the present paper is to explore the suitability of the new diffractometer for studying polymer fibres. The operation of the diffractometer will be demonstrated using data from fibres of polyethylene (PE) and polypropylene (PP), and then a specific application of the diffractometer to the meridional scattering from copolymers of poly(1,4-hydroxybenzoic acid) with poly(2,6-hydroxynaphthoic acid) will be discussed. Since the transformation of data from the CCD detector to reciprocal space is far from linear and relies upon the sample possessing uniaxial fibre symmetry, the effect of deviations from ideal fibre symmetry on the final appearance of the diffraction patterns will also be examined.

EXPERIMENTAL

Diffractometer design

Full details of the design of the new diffractometer have been published elsewhere[6]. Monochromatized $CuK_{\bar{\alpha}}$ radiation is used. The sample, which consists of a bundle of parallel fibres, is mounted in an Eulerian cradle, attached to the θ circle of a horizontal coupled $\theta - 2\theta$ goniometer. The Eulerian cradle allows control of the tilt-angle of the fibre, χ. The CCD detector is mounted on the 2θ arm of the goniometer and is housed on a refrigerated chamber. The choice of a CCD, rather than, for example, a multiwire position sensitive detector, was governed principally by cost. Many X-ray detectors based on CCD technology have now been developed[8–21], and a number are available commercially. We are using an X-ray sensitive video camera with an 18 mm diagonal aperture, made by Photonic

Science Ltd[10]. Similar cameras, with larger apertures, have also been used recently in novel X-ray systems by Keates *et al.*[22] and Mahendrasingham *et al.*[23]. The video signal from the CCD camera is fed into a frame-store, where it is integrated for the duration of each 'snapshot'. The frame-store and goniometer are controlled using a personal computer which also performs the subsequent image processing.

CCD operating conditions

The use of a sealed-beam X-ray source together with an incident beam monochromator results in a very low scattered X-ray flux, so that noise in the output from the CCD camera poses a significant problem. The main source of noise is thermal excitation of electrons in the CCD and image intensifier. The noise in the CCD can be overcome by setting a high gain factor on the image intensifier. However, thermal noise generated in the image intensifier itself can only be removed by lowering its temperature, which we achieve by placing the whole CCD camera in a refrigerated box at 3°C.

Data handling

The data obtained from the CCD require correction for inhomogeneities in the detector, before they may be used reliably. Fortunately, spatial aberrations are negligible due to the small entrance aperture. However, non-uniformities in detection sensitivity are a problem, and in the present case we find that the sensitivity varies from a maximum close to the centre of the detector to around 65% of the value at the corners. To compensate for this, the CCD pixel sensitivity has been calibrated and each image acquired is scaled before use. The calibration was performed by placing a point source of X-rays (a radioactive β source combined with a copper target) a large distance from the detector, and integrating the detected X-rays at each pixel for several hours. The illumination of the detector by the X-rays was assumed to be uniform. Further details may be found in ref. [6].

The transformation of intensity data from machine coordinates, i.e. the row and column number of each pixel (i,j) and goniometer angles, to reciprocal space coordinates, relies on the assumption that the sample has uniaxial fibre symmetry. This in turn implies that reciprocal space is averaged, cylindrically, about the reciprocal fibre axis, and can be described by an axial coordinate, Z, and a radial coordinate, R. The full transformation is as follows[6]:

$$R = \sqrt{\frac{2}{r\lambda^2}(r - d\cos 2\theta + x\sin 2\theta - Z^2)} \qquad (1)$$

$$Z = \frac{1}{r\lambda}(\sin\chi[(r+d)\sin\theta + x\cos\theta] + y\cos\chi)$$

where $r^2 = x^2 + y^2 + d^2$, $x = P_x(i - i_o)$ and $y = P_y(j - j_o)$. λ is the X-ray wavelength, d is the sample to detector distance (typically in the range 50–75 mm) and P_x and P_y are scale factors to convert the pixel coordinates(i,j) into metric units, relative to the centre of the detector at $(i_o j_o)$.

The effect of the transformation is illustrated in *Figure 1*, which shows the projection of the camera surface into reciprocal space for a number of different goniometer settings. Two main features of the transformation may be observed. The first is that, as the fibre tilt-angle, χ, is varied, the camera projection rotates in reciprocal space. The second feature is that the camera image splits when close to the Z-axis, a consequence of the Ewald sphere curvature.

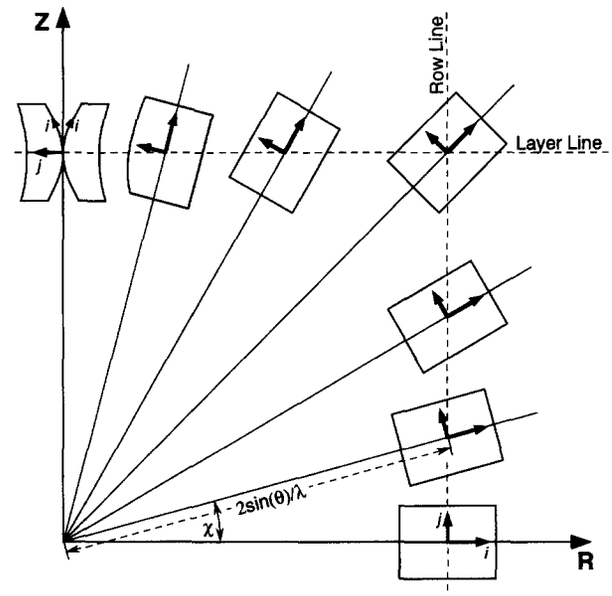

Figure 1 Illustration of the effect of projecting the camera coordinates into cylindrically averaged reciprocal space, while traversing an arbitrary layer line and row line. The features of the transformation are explained in the text. The fibre tilt angle, χ, becomes the azimuthal angle on the plot, Whereas the scattering angle, 2θ, is related to the radial distance from the origin, through the expression $R = 2\sin(\theta)/\lambda$

Therefore, for each dataset collected with the camera centred on the Z-axis, only a single point on the camera actually coincides with the Z-axis. This has implications for data collection which are discussed below.

Sample preparation

Samples of polyethylene and isotactic polypropylene were supplied by BP Chemicals. Polypropylene dumbells were cut from a 1.1 mm thick sheet made in a hot press at 230°C and cooled at 15°C min^{-1}. The dumbells were drawn at 110°C in an Instrom machine fitted with an air oven. A draw rate of 50 mm min^{-1} was used and the final draw ratio was 11. The polyethylene fibres were prepared in a similar way to the polypropylene ones, using a press temperature of 180°C and an oven temperature of 90°C. The final draw ratio in this case was 10. Samples of the liquid-crystalline copolymers of poly(1,4-hydroxybenzoic acid) with poly(2,6-hydroxynaphthoic acid) (B–N) were supplied by Hoechst-Celanese. Fibres with a nominal composition of 75 mol% benzoate units were hand-drawn from the melt at 300°C and annealed for 2 h at 215°C. All diffractometer samples consisted of a planar array of parallel fibres, of thickness between 0.3 and 0.4 mm.

RESULTS

Polypropylene

Figure 2a shows the fibre diffraction pattern from isotactic polypropylene. The pattern was formed from a superposition of 210 separate frames, each of which was integrated for 5 min, giving a total measurement time of approximately 17 h. The sample-to-film distance was 75 mm. The pattern has been constructed with a reciprocal space range from 0 to 0.85 $Å^{-1}$ and a resolution of 0.002 $Å^{-1}$ in both R and Z. The pattern was then reflected about the R and Z axes in order to show all

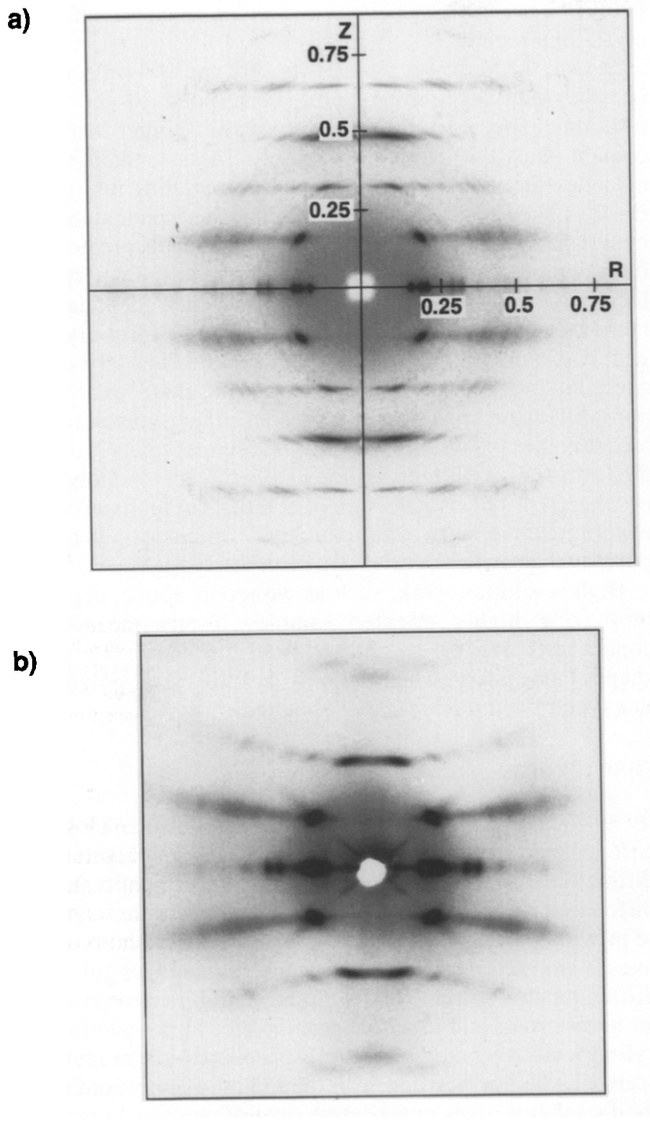

Figure 2 (a) Fibre diffraction pattern of polypropylene fibres created using the new diffractometer system. The R and Z axes are in units of $Å^{-1}$. (b) A normal incidence flat plate fibre photograph from the same sample for comparison. The equator and five layer lines are accessed in the diffractometer image compared with the equator and only three layer lines in the photograph

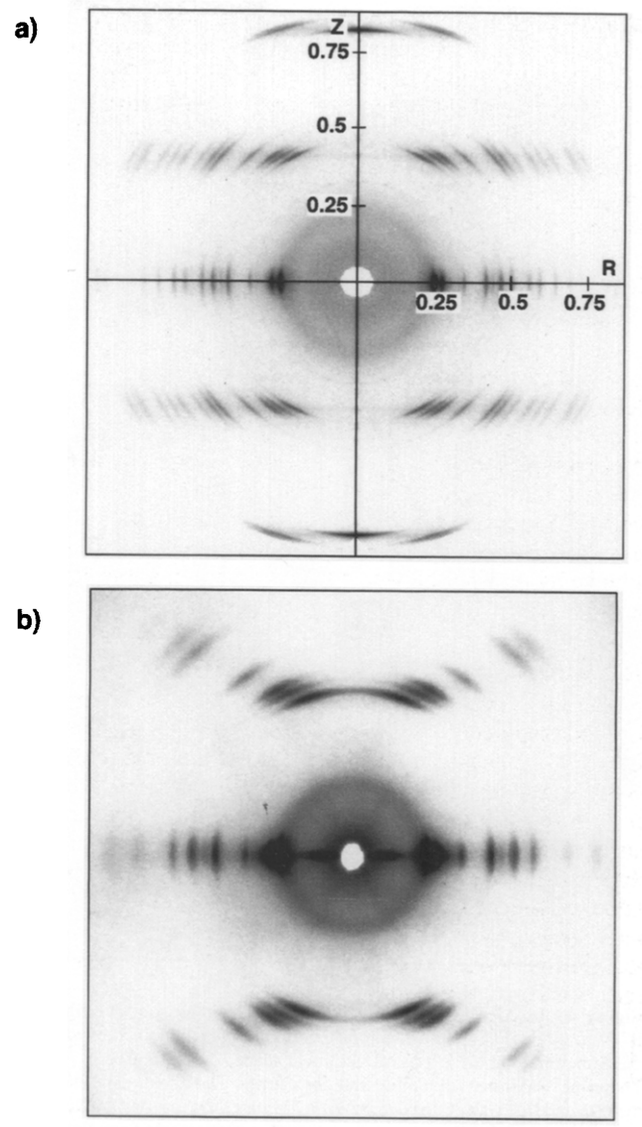

Figure 3 (a) Fibre diffraction pattern of polyethylene fibres from the new system, compared with (b) a normal incidence fibre photograph from the same sample. It can be seen that many more reflections are visible when using the diffractometer than can be seen in the photograph, including, on the meridian, the 002 reflection. The R and Z axes in (a) are in units of $Å^{-1}$

four quadrants. Five clear layer lines are visible in addition to the equatorial diffraction, compared with only three in the flat-plate photograph (*Figure 2b*). The diffraction pattern provides a striking example of one of the main advantages of the diffractometer, namely its ability to provide an undistorted image of reciprocal space, which manifests itself in the straight appearance of both the layer and row lines. The resulting image should be contrasted with the flat-plate photograph in *Figure 2b*, in which the layer and row lines are curved, and reflections close to the meridian are missing due to the Ewald sphere curvatures.

Polyethylene

The fibre diffraction pattern from the polyethylene sample is shown in *Figure 3*, with a standard normal incidence fibre photograph for comparison. The data were collected using the same measurement conditions as for polypropylene. Two layer lines are clearly visible, the second including the 002 reflection. This reflection cannot usually be seen on fibre photographs because of the Ewald sphere curvature. It is also interesting to note that there are twelve reflections extending to wide angles along the first layer line in the diffractometer image, of which only the first seven may be observed on the film. Profile fitting to these data, using the CCP13 suite of programs from Daresbury, has allowed extraction of integrated peak intensities, peak broadening factors and cell parameters. Variations in the intensities of these wide-angle reflections are currently being used to study subtle changes in the crystalline structure of the polyethylene chains from samples with varying branch content[24]. Such structural refinements would not be feasible using film data alone. It can also be seen that the reflections are arced, indicating an imperfect fibre orientation. A higher draw ratio was not chosen, however, because of possible disruption to the crystal structure. The significance of this arcing will be discussed in further detail below.

B–N copolymers

Figure 4 shows the meridian (i.e. the Z axis) of the fibre pattern from a sample of B–N containing 75 mol% of

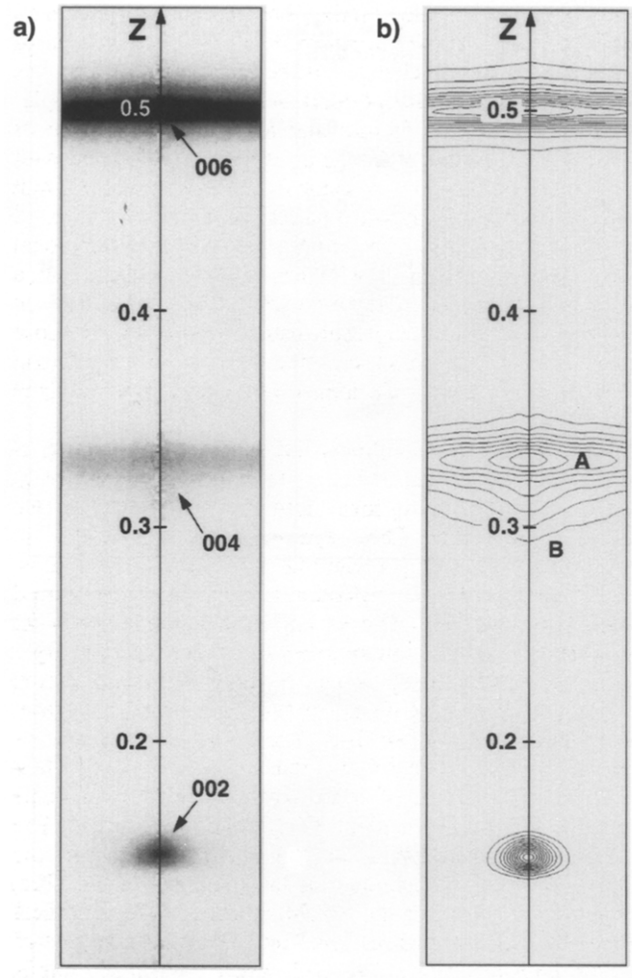

Figure 4 (a) Meridional diffractometer scan from an annealed fibre of a B–N copolymer containing 75 mol% benzoate units, obtained by stepping the detector along the Z axis of reciprocal space. Z is measured in $Å^{-1}$. (b) The same scan after smoothing and contouring. The asymmetric nature of the 002 and 004 reflections can be seen. The laterally broader, higher angle part of the 004 reflection, labelled as **A**, is thought to come from the poorly registered non-crystalline component of the polymer, while the narrower lower angle part, labelled as **B**, is thought to come from the crystalline component. The difference in scattering vector for the two parts of the reflection is thought to depend on the different compositions of the crystalline and non-crystalline components

benzoate units. We have superimposed approximately 200 datasets of 5 min duration, moving the detector along the meridian in equal steps of 0.002 $Å^{-1}$. This surprisingly large number of datasets was needed because only one point actually lies on the Z axis, *per* dataset, as mentioned above. The *00l* reflections, with their characteristic aperiodic positions[25,26], are readily seen.

In fact, it can be seen from *Figure 4* that the 002 and 004 reflections are asymmetric on shape along the Z axis. The 004 reflection has a pronounced low angle tail, where the reflection becomes narrower laterally, and 002 has a similar, though less marked, high angle tail. The peak shapes are consistent with recent predictions from crystallization models for the B–N copolymers[27]. The aperiodic positions of the *00l* reflections are a consequence of the randomness of the monomer sequences along the polymer chains, and depend on the monomer composition of the copolymer. The lateral width of the *00l* reflections indicates the degree of registration between adjacent polymer molecules. Thus, laterally narrower reflections correspond to regions of the polymer possessing better molecular registration, i.e. crystalline regions.

In fact, the narrower parts of the 002 and 004 reflections, i.e. the more crystalline parts, correspond to the peak positions expected for copolymers with a higher benzoate content than the sample possesses. This is taken to be evidence that the composition of the crystalline regions of B–N is skewed towards the dominant component of the material, an observation which is in line with predictions from computer models of non-periodic layer (NPL) crystallites[28]. NPL crystallites are crystals in which identical but random sequences of monomers coalesce to form crystals with two-dimensional periodicity perpendicular to the chain axes, but no periodicity parallel to the chain axes. Our preliminary findings appear to lend further support to the idea that the crystallinity found in B–N copolymers is due to the formation of NPL crystallites, rather than homopolymer, or other, types of crystal. A more detailed comparison of the experimental results with computer simulation is to be published elsewhere.

High resolution work, such as we report above, depends on having highly oriented samples if any meaningful conclusions are to be drawn from the observed peak shapes.Fortunately, when studying liquid-crystal polymers, this type of sample is readily obtained.

DISCUSSION

Advantages and disadvantages of the new diffractometer

It is clear from the above results that the CCD-based fibre diffractometer is capable of generating good quality X-ray diffraction data. However, it is important for the new system to provide more information than traditional methods, if its use is to be justified. The main advantages of *any* diffractometer system over film, are its ability to produce an undistorted, and essentially complete, representation of cylindrically averaged reciprocal space, up to the maximum scattering vector possible with the radiation employed, and the fact that it gives quantitative intensities.

The advantage of using a CCD detector is the improvement in measurement time over a conventional detector, which, in practice, allows an improvement in resolution. In fact, in the examples shown above, the total data collection times are comparable to those previously used for oriented amorphous polymers[2,4], but with an improvement in resolution by a factor of ≈ 10 in both R and Z. The benefits, when examining subtle variations in the positions, shapes and intensities of reflections, are clear. In the worst case, when studying diffraction features on the Z axis of reciprocal space, measurement times will be comparable for both types of detector, but the CCD simultaneously provides extra information, close to the Z axis, which a point-detector does not, as was demonstrated by the results for the B–N copolymers (see *Figure 4*).

The maximum resolution of the diffractometer is governed by the CCD camera, and depends on the pixel size and the camera optics. We find that we obtain an angular resolution of around $0.03°2\theta$ under typical operating conditions. Since the camera is scanned in 2θ, there is *no* trade-off between angular range and angular resolution, which is a limitation of systems with stationary detectors. Instead, we are always able to work at maximum resolution.

Orientation effects

When examining the formation and overall integrity of the final diffraction image, it is important to consider the

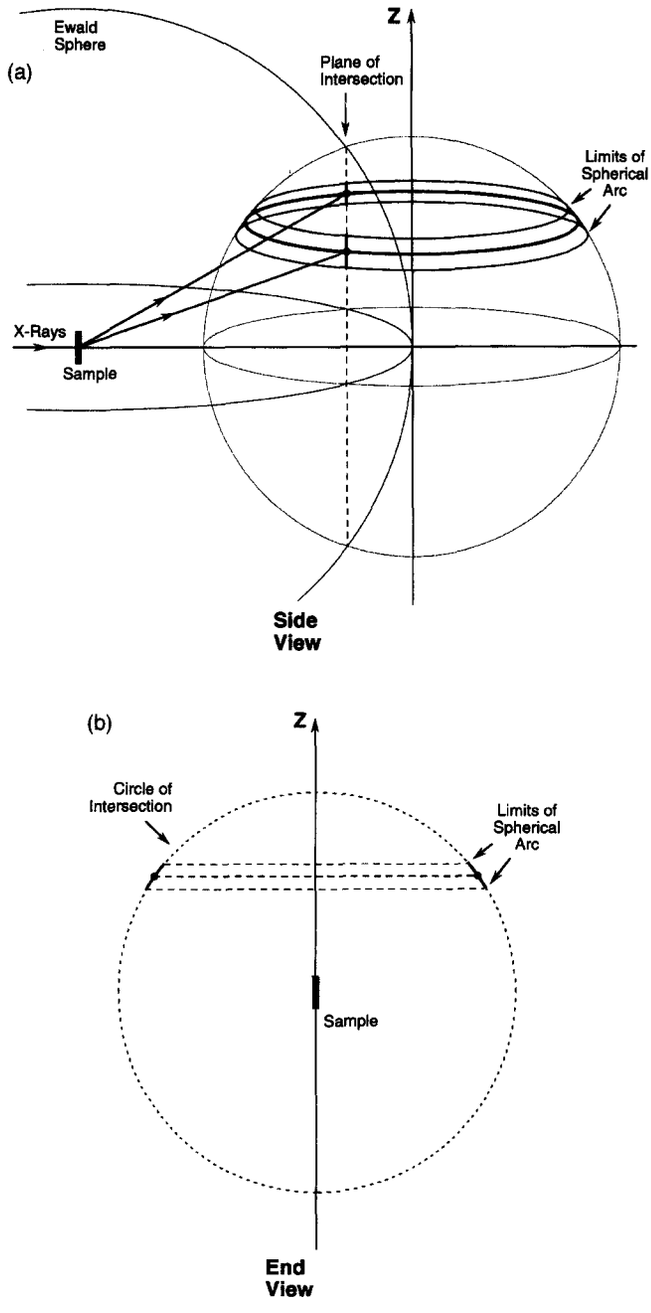

effects of misorientation on the fibre. Initial experiments on poorly oriented samples *appeared* to show that the radius of each arced reflection changed as the goniometer setting was changed. It should be pointed out that, with a sample-detector distance of 50 mm and an entrance aperture of 18 mm, it is possible to image an equatorial reflection with the camera centred on 2θ values up to 10° apart. At first sight, it was not clear how the pattern from a poorly oriented fibre would transform from camera coordinates to reciprocal space coordinates, and whether, indeed, images of a particular reflection, obtained with the CCD centred on different points in reciprocal space, would superimpose correctly. This was an important consideration when trying to measure accurate peak intensities from the polyethylene sample in *Figure 3*.

To examine what actually happens when looking at poorly oriented fibres, one may use a similar argument to that used for discussing ideal fibre symmetry. That is, one may imagine that fibre symmetry is equivalent to cylindrically averaging reciprocal space about the Z axis, so that each crystalline reflection becomes a circle centred on the Z axis. In the ideal case, any intersection between the circle and the Ewald sphere gives rise to a reflection. By a similar argument, the presence of uniaxial misorientation leads to the formation of a spherical arc in reciprocal space, as illustrated in *Figure 5a*.* Since two spheres always intersect in a circle, it follows that the observed reflection must be in the form of a circular arc, lying in a plane perpendicular to the incident X-ray beam (*Figure 5b*). The radius of the arc depends on the scattering angle of the reflection, but is independent of the tilt angle of the fibre, because the centres of the Ewald sphere and the spherical arc are fixed in the construction. Thus, although the radius of the arc *appears* different in each X-ray 'snapshot', this is simply due to there being a different projection onto camera coordinates in each case, because there is an angle of 2θ between the plane of the arc and the plane of the camera surface. In fact, since the reciprocal space transformation (equation (1)) was derived for *any* cylindrically symmetric diffraction intensity, it is clear that all images of a particular reflection *must* superimpose correctly, so that the final diffraction pattern will consist of a set of concentric arcs, centred on the origin, as illustrated for polyethylene in *Figure 5c*. Furthermore, by an extension to this argument, we may see that, if the sample is completely lacking in orientation, the diffraction pattern will appear as a set of concentric rings, just as in a simple transmission X-ray photograph. In this case, spherical symmetry may be regarded as a special case of uniaxial symmetry. It is clear, therefore, that the diffractometer may be relied upon to give accurate peak intensities for *any* uniaxial orientation distribution.

* By a 'spherical arc' we mean the three-dimensional shape obtained by revolving an arc of a circle about an axis in the plane of the circle. It might alternatively be thought of as a parallel sided slice through a spherical shell.

Figure 5 (a) Ewald sphere construction for a cylindrically averaged fibre with poor orientation. Each reflection takes the form of a spherical arc. (b) The intersection of the spherical arc in (a) with the Ewald sphere results in a circular arc, whose radius will depend only on the scattering angle, and not on the tilt of the fibre. (c) Diffraction pattern from the polyethylene sample of *Figure 3*a with circles drawn in to emphasize the fact that each reflection is correctly shown as a circular arc

However, if the fibre does not possess uniaxial symmetry, for example if it is biaxial, the situation is rather different. Now, if the same reflection is imaged using several different goniometer settings, the CCD will 'see' a different orientation distribution in each case. Thus, although each image of an arced reflection will still have the same radius and will superimpose correctly, each will have a different azimuthal width, and it will be impossible to obtain a reliable estimate of the integrated intensity. Therefore, the new diffractometer will be unsuitable for studying non-uniaxial samples, unless one has a very clear *a priori* knowledge of their orientation distributions.

CONCLUSIONS

We have described the application of a new CCD-based diffractometer to studies of crystalline and liquid crystalline polymer fibres. The main advantages of the new system are its ability to display a high-resolution, undistorted view of reciprocal space, to access reflections close to the meridian, and to perform quantitative intensity measurements. It offers a significant improvement in measurement time compared to diffractometers with conventional detectors, which, in practice, allows higher resolution measurements to be performed. The new machine is best suited to studying fibres with uniaxial symmetry, in which case reliable integrated intensities of crystalline reflections may be found, irrespective of the degree of orientation. If the sample is very highly oriented, subtleties of peak shapes and diffuse scattering may be studied. In the case of the B–N copolymer, the new diffractometer has allowed the shapes of the *00l* reflections to be observed and related to predictions from the NPL model of crystallinity. The diffractometer is less well suited to the study of biaxially oriented polymers.

ACKNOWLEDGEMENTS

The authors would like to thank the EPSRC for a grant, the EPSRC and BP Chemicals for a CASE studentship and Prof. C.J. Humphreys for the provision of laboratory space. They are grateful for the technical assistance of Messrs Brian Seymour, John Carter and Joe Ellis during the development of the diffractometer. They also wish to thank Drs Paul Gibson, Kenn Gardner and U. Arndt for helpful discussions.

REFERENCES

1. Mckie, D. and Mckie, C., *Essentials of Crystallography*. Blackwell Scientific Publications, Oxford, 1986, pp. 252–264.
2. Lovell, R. and Windle, A. H., *Polymer*, 1976, **17**, 488–494.
3. Lovell, R. and Windle, A. H., *Acta Cryst.*, 1977, **A33**, 390–395.
4. Arndt, U. W., *J. Appl. Cryst.*, 1986, **19**, 145–163.
5. Arndt, U. W., *Synchrotron Radiation News*, 1990, **3**, 17–22.
6. Hanna, S. and Windle, A. H., *J. Appl. Cryst.*, 1995, **28**, 673–689.
7. Hanna, S. and Windle, A. H., *Advances in X-Ray Analysis*, 1995, **38**, 503–510.
8. Elf, F., Will, G. and Weisgerber, S., *Materials Science Forum*, 1991, 79–82, 371–376.
9. Widom, J. and Feng, H. P., *Rev. Sci. Instrum.*, 1989, **60**, 3231–3238.
10. Tomkins, P. R., *Adv. Electron. and Electron Phys.*, 1988, **74**, 27–33.
11. Templer, R. H., Gruner, S. M. and Eikenberry, E. F., *Adv. Electron and Electron Phys.*, 1988, **74**, 275–283.
12. Van Geest, L. K., *Adv. Electron. and Electron Phys.*, 1988, **74**, 1–8.
13. Eikenberry, E. F., Gruner, S. M. and Lowrance, J. L., *IEEE Trans. Nucl. Sci.*, 1986, **83**, 542–545.
14. Nakajima, K., Sudo, S. and Aoki, S., *Japanese J. Appl. Phys. 1*, 1993, **32**, 5754–5758.
15. Moy, J. P., *Nucl. Instrum. Methods A*, 1994, **348**, 641–644.
16. Rodricks, B., Huang, Q., Hopf, R. and Wang, K. M., *Nucl. Instrum. Methods A*, 1994, **348**, 572–576.
17. Tate, M. W., Eikenberry, E. F., Barna, S. L., Wall, M. E., Lowrance, J. L. and Gruner, S. M., *J. Appl. Cryst.*, 1995, **28**, 196–205.
18. Huang, Q., Hopf, R. and Rodricks, B., *Nucl. Instrum. Methods A*, 1994, **348**, 645–648.
19. Moon, K. J., Allinson, N. M. and Helliwell, J. R., *Nucl. Instrum. Methods A*, 1994, **348**, 631–634.
20. Kock, A., *Nucl. Instrum. Methods A*, 1994, **348**, 654–658.
21. Naday, I., Westbrooke, E. M., Westbrooke, M. L., Travis, D. J., Stanton, M., Phillips, W. C., O'Mara, D. and Xie, J., *Nucl. Instrum. Methods A*, 1994, **348**, 635–640.
22. Keates, P., Mitchell, G. R., Peuvrel-Disdier, E. and Navard, P., *Polymer*, 1993, **34**, 1316–1319.
23. Mahendrasingham, A., Martin, C., Jaber, A., Hughes, D., Fuller, W., Rule, R., Oldman, R. J., Mackerron, D. and Blundell, D. J., *Nucl. Instrum. Methods B*, 1995, **97**, 238–241.
24. Baker, A. M. E. Ph.D. Thesis, University of Cambridge, UK, 1996.
25. Windle, A. H., Viney, C., Golombok, R., Donald, A. M. and Mitchell, G. R., *Faraday Discuss. Chem. Soc.*, 1985, **79**, 55–78.
26. Gutierrez, G. A., Chivers, R. A., Blackwell, J., Stamatoff, J. B. and Yoon, H., *Polymer*, 1983, **24**, 937–942.
27. Hanna, S., Hurrell, B. L., Windle, A. H., in *Crystallisation of Polymers*, ed. M. Dosière. Kluwer Academic Publishers, Dordrecht, 1993, pp. 559–564.
28. Hanna, S. and Windle, A. H., *Polymer*, 1988, **29**, 207–223.